LETTER

https://doi.org/10.1038/s41586-019-1162-y

Prophylactic TNF blockade uncouples efficacy and toxicity in dual CTLA-4 and PD-1 immunotherapy

Elisabeth Perez-Ruiz[1,2,3,4,5], Luna Minute[1,2], Itziar Otano[1,2], Maite Alvarez[1,2], Maria Carmen Ochoa[1,2,6], Virginia Belsue[1,2], Carlos de Andrea[2,7], Maria Esperanza Rodriguez-Ruiz[1,3], Jose Luis Perez-Gracia[2,3,6], Ivan Marquez-Rodas[6,8], Casilda Llacer[9], Martina Alvarez[5,10,11], Vanesa de Luque[5,10], Carmen Molina[1,2], Alvaro Teijeira[1,2,6], Pedro Berraondo[1,2,6,13]* & Ignacio Melero[1,2,3,6,12,13]*

Combined PD-1 and CTLA-4-targeted immunotherapy with nivolumab and ipilimumab is effective against melanoma, renal cell carcinoma and non-small-cell lung cancer[1–3]. However, this comes at the cost of frequent, serious immune-related adverse events, necessitating a reduction in the recommended dose of ipilimumab that is given to patients[4]. In mice, co-treatment with surrogate anti-PD-1 and anti-CTLA-4 monoclonal antibodies is effective in transplantable cancer models, but also exacerbates autoimmune colitis. Here we show that treating mice with clinically available TNF inhibitors concomitantly with combined CTLA-4 and PD-1 immunotherapy ameliorates colitis and, in addition, improves anti-tumour efficacy. Notably, TNF is upregulated in the intestine of patients suffering from colitis after dual ipilimumab and nivolumab treatment. We created a model in which *Rag2*$^{-/-}$*Il2rg*$^{-/-}$ mice were adoptively transferred with human peripheral blood mononuclear cells, causing graft-versus-host disease that was further exacerbated by ipilimumab and nivolumab treatment. When human colon cancer cells were xenografted into these mice, prophylactic blockade of human TNF improved colitis and hepatitis in xenografted mice, and moreover, immunotherapeutic control of xenografted tumours was retained. Our results provide clinically feasible strategies to dissociate efficacy and toxicity in the use of combined immune checkpoint blockade for cancer immunotherapy.

Treatment with the anti-PD-1 monoclonal antibody nivolumab in combination with the anti-CTLA-4 monoclonal antibody ipilimumab produces synergistic immunotherapeutic effects in patients who are affected by a variety of cancers[1–4]. Following convincing evidence on the efficacy of combined CTLA-4 and PD-1 blockade in mouse models of cancer[5–8], a phase I dose-escalation clinical trial was conducted in patients with metastatic cutaneous melanoma. This resulted in clinical responses that were frequent, strong and sustained over time[4]; however, over 40% of patients suffered serious immune-related adverse events, necessitating a reduction in the dose of ipilimumab in the recommended combination regimens for phase II trials[9]. In the phase I trial, one cohort of six patients with melanoma was given a biweekly dose of 3 mg kg^{-1} nivolumab together with 3 mg kg^{-1} ipilimumab; all six experienced marked clinical responses but the treatment had to be stopped because of dose-limiting toxicity[4]. Moreover, evidence from a randomized phase III trial of patients with melanoma indicated that a dose of 10 mg kg^{-1} of ipilimumab alone every three weeks resulted in longer overall survival than a regimen with 3 mg kg^{-1} of ipilimumab alone[10].

Immune-related adverse events that result from therapy with checkpoint inhibitors are usually satisfactorily treated by discontinuing the use of the therapeutic agents and beginning a course of steroids[11]. TNF blockade with infliximab is recommended for cases that are serious or are refractory to steroids[11]—with the exception of patients with hepatitis, because of the putative role of TNF in promoting liver regeneration[12]. In this study, we provide evidence that the prophylactic blockade of TNF before the start of dual anti-CTLA-4 and anti-PD-1 therapy prevents autoimmune adverse events in mouse models, and also enhances to some extent the anti-tumour efficacy of the combined treatment.

Colitis is among the most frequent and problematic immune-mediated adverse events that are associated with dual checkpoint inhibition[11]. Inflammatory bowel disease can be modelled in mice by providing dextran sulfate sodium (DSS) in the drinking water[13,14]. We performed a series of experiments in which a combination of anti-CTLA-4 and anti-PD-1 monoclonal antibodies (Fig. 1a) was administered to mice receiving DSS. The combination treatment exacerbated the autoimmune colitis syndrome induced by DSS and resulted in weight loss (Fig. 1b), a thickening of the wall of the large intestine (as detected by ultrasound; Fig. 1c, d) and worsening of colon inflammation (as assessed by histological techniques; Fig. 1e). TNF blockade is a recommended treatment for ulcerative colitis[15] and Crohn's disease. Prophylactic administration of the monoclonal antibody anti-mouse TNF or the TNF inhibitor etanercept (TNFR2–IgG)[16] clearly ameliorated the treatment-induced worsening of DSS-induced colitis (Fig. 1a–d).

We next studied whether prophylactic TNF blockade would affect the anti-tumour activity of the anti-PD-1 and anti-CTLA-4 combination in mice with established MC38 or B16-ovalbumin (OVA)-derived tumours. Inhibition of TNF with a specific monoclonal antibody or etanercept did not impair the anti-tumour effects of dual checkpoint inhibition against MC38-derived tumours (Fig. 2a–c), and similar observations were made for B16-OVA-derived melanomas (Extended Data Fig. 1). These data indicate that TNF functions are dispensable and, to some extent, harmful to the anti-tumour activities of the combined immunotherapy regimens. In parallel experiments, we also attempted preventive blockade of IL-6, as previous reports suggested that neutralization of IL-6 could be a potential cancer treatment[17,18]. However, in our case, anti-tumour efficacy was partially reduced in the MC38 and B16-OVA models (Extended Data Fig. 2). Notably, the TNF-neutralizing agents resulted in a higher fraction of mice that completely rejected their tumour grafts, as compared with mice that were also treated with double checkpoint

[1]Program of Immunology and Immunotherapy, Cima Universidad de Navarra, Pamplona, Spain. [2]Navarra Institute for Health Research (IDISNA), Pamplona, Spain. [3]Department of Oncology, Clínica Universidad de Navarra, Pamplona, Spain. [4]Department of Oncology, Hospital Costa del Sol, Marbella, Spain. [5]Instituto de Investigación Biomédica de Málaga (IBIMA), Hospitales Universitarios Regional y Virgen de la Victoria, Málaga, Spain. [6]Centro de Investigación Biomédica en Red de Cáncer (CIBERONC), Madrid, Spain. [7]Department of Pathology, Clínica Universidad de Navarra, Pamplona, Spain. [8]Department of Oncology, Hospital General Universitario Gregorio Marañon, Madrid, Spain. [9]Department of Oncology, Hospital Universitario Virgen de la Victoria, Málaga, Spain. [10]Laboratorio de Biología Molecular del Cáncer, Centro de Investigaciones Médico-Sanitarias (CIMES), Universidad de Málaga, Málaga, Spain. [11]Department of Pathology, Faculty of Medicine, Universidad de Málaga, Málaga, Spain. [12]Department of Immunology and Immunotherapy, Clínica Universidad de Navarra, Pamplona, Spain. [13]These authors jointly supervised this work: Pedro Berraondo, Ignacio Melero. *e-mail: pberraondol@unav.es; imelero@unav.es

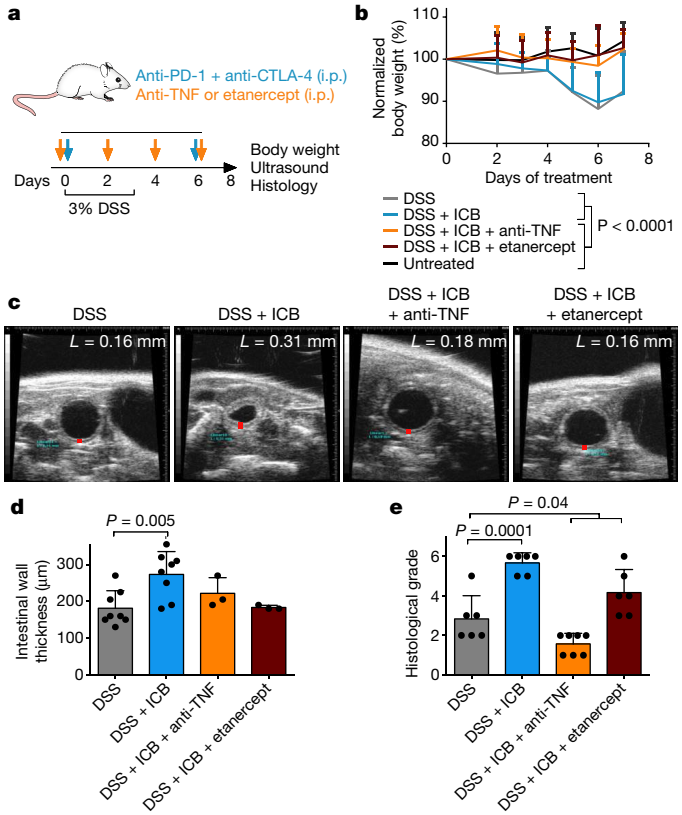

Fig. 1 | DSS-induced colitis, exacerbated by anti-PD-1 and anti-CTLA-4, is ameliorated by prophylactic TNF blockade. a, Mice with DSS-induced colitis were treated intraperitoneally (i.p.) with anti-PD-1 and anti-CTLA-4 monoclonal antibodies, either in combination with TNF blockade (using anti-TNF monoclonal antibodies or etanercept) or without TNF blockade. **b**, Normalized follow-up of body weight as a surrogate indicator of colitis severity in mice. Data are mean ± s.d. $n = 9$ biologically independent mice. *P* value was calculated using an extra sum-of-squares *F* test. ICB, immune checkpoint blockade. **c**, **d**, Representative ultrasound assessments (**c**) and quantification (**d**) of intestinal wall thickness. Red bars in **c** indicate wall thickness. *L*, quantification of intestinal wall thickness. Data are mean ± s.d. $n = 8$ biologically independent mice for DSS and DSS + ICB; $n = 3$ for the groups treated with anti-TNF or etanercept. *P* value was calculated using a one-way analysis of variance (ANOVA) followed by Dunnett's test. **e**, Quantification of the severity of colon wall inflammation in haemotoxylin and eosin (H&E)-stained sections. Histological grade was evaluated by a clinical pathologist blinded to the origin of samples. Data are mean ± s.d. $n = 7$ biologically independent mice for the groups treated with anti-TNF or etanercept; $n = 6$ for the other groups. *P* values were calculated using a one-way ANOVA followed by Dunnett's test. Data are pooled from two independent experiments.

inhibition but without prophylactic TNF blockade (Fig. 2). These data may be in line with a previous study, which reported that tumour-bearing mice that were either genetically deficient in TNF or subjected to TNF blockade responded slightly better to anti-PD-1 single-agent treatment[19].

We next sought to determine whether the enhancement of anti-tumour effects would also occur in MC38 tumour-bearing mice in which colitis had been concomitantly induced by DSS. Mice that received etanercept or anti-TNF monoclonal antibody in addition to double checkpoint blockade had an advantage in tumour rejection and survival over mice that received double checkpoint blockade alone (Fig. 2d–f). The neutralizing antibody was more consistently effective than etanercept, possibly owing to the fact that immune-competent mice develop anti-drug antibodies more efficiently in response to etanercept than to the anti-TNF antibody (Extended Data Fig. 3). In addition, combined anti-CTLA-4 and anti-PD-1 treatment increased TNF concentrations in the tumour microenvironment, but TNF was undetectable in serum samples from the same mice (Extended Data Fig. 4), and perhaps for this reason the better tissue penetration of the anti-TNF monoclonal antibody is preferable to that of etanercept.

Double checkpoint inhibition in mice with MC38 or B16-OVA tumours led to an increase in $CD8^+$ T cells in the tumour infiltrate, and this was further enhanced by anti-TNF or etanercept treatment (Extended Data Fig. 5a). A similar increase was evident for tumour antigen-specific $CD8^+$ T cells in the tumour microenvironment and tumour-draining lymph nodes, as detected by immunostaining with gp70 H-$2K^b$ pentamer (Fig. 3a, b).

We investigated whether the beneficial anti-tumour effects of prophylactic TNF blockade could be related to the reversion of an exhaustion phenotype of $CD8^+$ T cells. MC38 tumour-infiltrating $CD8^+$ T cells that were subjected to double checkpoint blockade and TNF inhibition with either a neutralizing monoclonal antibody or etanercept had a lower surface expression of PD-1 (Extended Data Fig. 5b, d), as assessed by a non-competing anti-PD-1 monoclonal antibody[20]. We also looked specifically at surface TIM3 expression on tumour-specific tumour-infiltrating $CD8^+$ T cells, as a result of a previous report[19] in which TNF blockade led to a decrease in TIM3 expression after anti-PD-1 single-agent treatment—the enhanced efficacy of the anti-PD-1 treatment in combination with TNF blockade was attributed to this decrease. By contrast, in our study, the surface expression of TIM3 was not modified by double checkpoint blockade either alone or in combination with TNF blockade (Extended Data Fig. 5c). We also tested a wide panel of molecules that are associated with T-cell exhaustion, and found no discernible changes—other than the reduction in PD-1—that could be attributed to the TNF blockade (Extended Data Fig. 6). The reduction in surface PD-1 did not result from internalization[20]; instead, it probably involved the selective expansion, on treatment, of $CD8^+$ T cells that express little or no PD-1, as has been recently reported[21,22].

Another mechanistic possibility for the enhanced anti-tumour effects is the attenuation of activation-induced cell death (AICD) in T lymphocytes[23]. Indeed, mouse T cells that are deficient in TNFR1 (*Tnfrsf1a*$^{-/-}$) reportedly undergo considerably higher levels of AICD[24]. In keeping with this finding, we observed that TNF blockade with anti-TNF or etanercept decreased apoptosis in T cell-receptor (TCR)-transgenic mouse $CD8^+$ OT-I and Pmel-1 cells activated in culture with their respective cognate peptides in the presence of anti-PD-1 and anti-CTLA-4 monoclonal antibodies (Fig. 3c, d). Furthermore, in mice bearing MC38 tumours and suffering from DSS-induced colitis that were treated with double checkpoint blockade, systemic neutralization of TNF resulted in increased viability of tumour-reactive $CD8^+$ T cells in the tumour microenvironment (Fig. 3e) and even more prominently so in tumour-draining lymph nodes (Fig. 3f). Notably, human $CD8^+$ T lymphocytes—from healthy donors—that were activated with anti-CD3 and anti-CD28 monoclonal antibodies underwent less AICD when cultured in the presence of infliximab (an anti-TNF monoclonal antibody) or etanercept (Fig. 3g, Extended Data Fig. 7).

To address the clinical applicability of these mouse data, we investigated whether the TNF pathway is turned on in patients with cancer who developed colitis upon checkpoint blockade. We analysed the mRNA expression of immune-related genes in sections of healthy mucosal tissue from colon biopsies of patients who either had checkpoint-induced colitis or had been diagnosed with bona fide ulcerative colitis (Fig. 4a, b). In all four cases of checkpoint-induced colitis that we tested, *TNF* mRNA expression was augmented, although it did not reach the level found in naturally occurring inflammatory bowel disease (Fig. 4a). The gene expression analyses were also consistent with transcripts reflecting local activation of the TNF gene signature (Fig. 4b). As TNF can be effectively targeted in

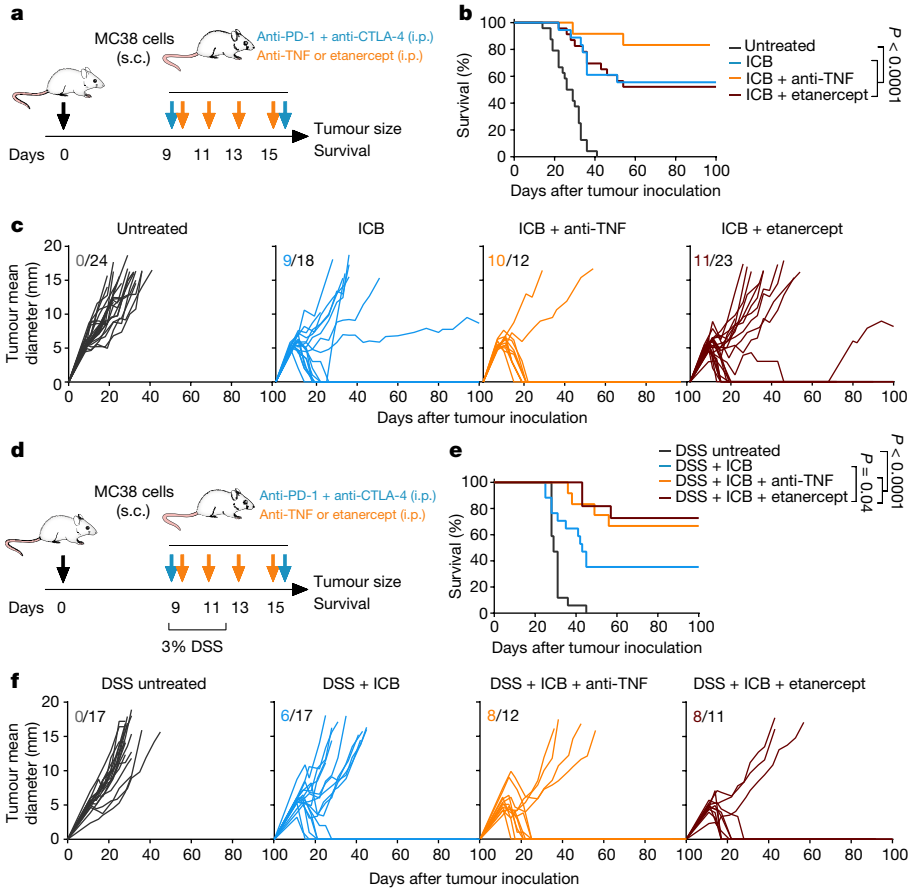

Fig. 2 | Prophylactic TNF blockade does not hinder—and even enhances—the anti-tumour activity of combined anti-PD-1 and anti-CTLA-4 immunotherapy. a, Schematic representation of the treatments applied to mice that were subcutaneously (s.c.) engrafted with MC38 colon carcinoma cells. **b**, Overall survival of the indicated treatment groups. The numbers of biologically independent mice are indicated in **c**. *P* values were calculated using a two-sided log-rank test. **c**, Individual follow-up of mean tumour diameters, depicting the fraction of mice that completely rejected established tumours. **d**, Schematic representation of experiments performed as in **a**, but with colitis induced from day 9 by providing DSS in the drinking water. **e**, **f**, As **b**, **c** but for mice with DSS-induced colitis. The numbers of biologically independent mice are indicated in **f**. *P* values were calculated using a two-sided log-rank test. Data are pooled from three independent experiments.

ulcerative colitis, it makes sense that blocking this cytokine could also prevent or attenuate double checkpoint-induced colitis, given that TNF is upregulated in situ in the intestinal lesions of patients with this condition.

To further explore the applicability of our findings, we used a xenograft-versus-host model of disease, in which human peripheral blood mononuclear cells (PBMCs) were infused into *Rag2*$^{-/-}$*Il2rg*$^{-/-}$ mice. This condition causes the inflammation of several target organs, including the colon[25]. Treating these mice with combined ipilimumab and nivolumab exacerbated the disease and resulted in reduced body weight compared with animals that were prophylactically co-treated with etarnercept (Extended Data Fig. 8a). In this setting of multi-organ autoimmunity exacerbated by double checkpoint blockade, etanercept—but not control human IgG—reduced inflammation in the large intestine (as assessed by ultrasound examinations of intestinal wall thickness; Extended Data Fig. 8b, c). We also subcutaneously xenografted HT29 colon cancer cells into our humanized mouse model (Fig. 4c), and observed that tumour progression was controlled to some extent by dual nivolumab and ipilimumab treatment. Concomitant etanercept treatment did not diminish these therapeutic effects (Fig. 4d). Moreover, xenograft-versus-host-induced hepatitis and colitis were markedly reduced in etanercept-treated mice (Fig. 4e–g).

TNF blockade is not new in the arena of cancer immunotherapy. A previous study[26] led to two clinical trials that tested etanercept and infliximab for the treatment of ovarian[27] and renal[28] cancer, respectively. Although the observed clinical activity in these trials was modest and not sufficient to warrant further clinical research, there was no reported evidence of disease hyper-progression. This suggests that TNF inhibition may constitute a safe treatment option in patients with advanced cancer.

On the basis of these results, together with our previous work, we propose that a sufficiently statistically powered phase II clinical trial should be conducted in which patients undergoing dual ipilimumab and nivolumab treatment are also administered an approved anti-TNF agent, prophylactically or concomitantly with the immunotherapy regimen. A phase I investigator-initiated trial testing the safety of this combined approach is currently in progress (https://clinicaltrials.gov; NCT03293784), and we suggest that this should be followed by a larger clinical trial that examines both safety (measured as the percentage of immune-related adverse events that are of grade 2 or higher) and objective activity (measured as the percentage of overall response rate in patients). Our results indicate that an anti-TNF agent may— at least in the gut and in the liver—improve the safety of combined ipilimumab and nivolumab immunotherapy, as well as equalling or perhaps enhancing its efficacy. If this hypothesis is correct, prophylactic TNF blockade might allow doses of ipilimumab to be safely increased in combined immune checkpoint blockade regimens, thereby potentially strengthening their anti-tumour effects.

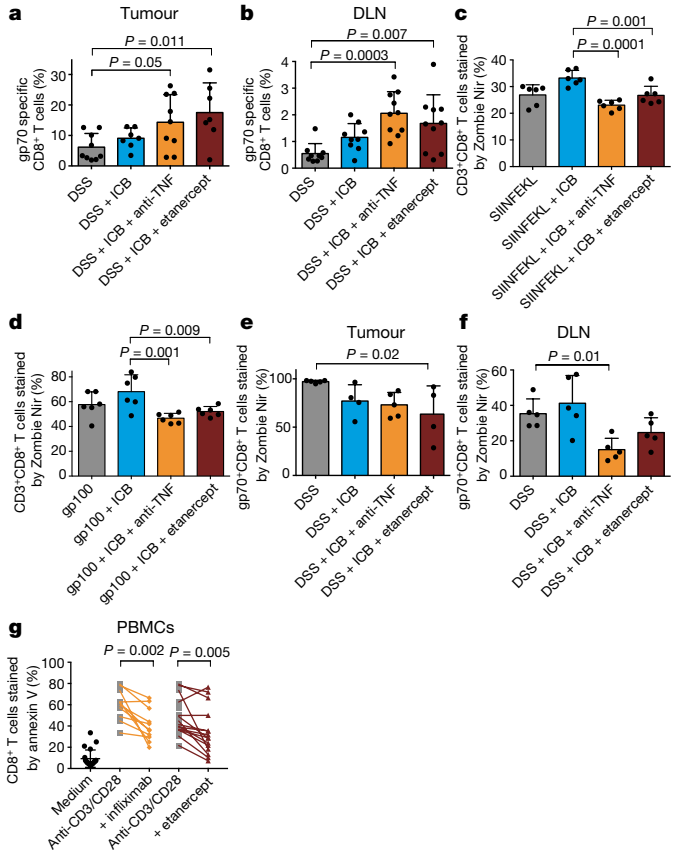

Fig. 3 | TNF blockade increases the infiltration of tumour-specific T cells in MC38-derived tumours and decreases AICD in CD8$^+$ T cells from mice and humans. Mice bearing MC38 tumours were treated as in Fig. 2d and killed on day 16. **a**, Tumour-specific CD8$^+$ T cells in the tumour microenvironment. $n = 9$ biologically independent mice for DSS and DSS + ICB + anti-TNF; $n = 7$ for DSS + ICB and DSS + ICB + etanercept. **b**, Tumour-specific CD8$^+$ T cells in the tumour draining lymph nodes (DLN). $n = 9$ for DSS and DSS + ICB; $n = 10$ for the groups treated with anti-TNF or etanercept. **c**, OT-I CD8$^+$ T cells were activated with cognate SIINFEKL peptide (25 ng ml^{-1}). Anti-PD-1 and anti-CTLA-4 monoclonal antibodies (6.6 μg ml^{-1}) were added to the ICB-treated cultures, and simultaneously anti-TNF (8.3 μg ml^{-1}) or etanercept (2.6 μg ml^{-1}) were added to the indicated conditions. Cell death was monitored by Zombie Nir staining of T cells after 72 hours. $n = 6$ biologically independent samples. **d**, Experiments were performed as in **c**, but with Pmel-1 T cells that were activated with 500 ng ml^{-1} of cognate gp100 peptide. $n = 6$ biologically independent samples of cells. Data are pooled from two independent experiments (**a**–**d**). **e**, **f**, Mice bearing MC38 tumours were treated as in **a**, and the fraction of viable gp70-reactive CD8$^+$ T cells was assessed by viability-dye exclusion in gated CD8$^+$ T cells from cell suspensions that were derived from either tumour-infiltrating lymphocytes (**e**) or tumour draining lymph nodes (**f**). $n = 5$ biologically independent mice for DSS and DSS + ICB + anti-TNF; $n = 4$ for DSS + ICB and DSS + ICB + etanercept. One representative experiment out of three is shown (**e**, **f**). Data are mean ± s.d; *P* values were calculated using a one-way ANOVA followed by Dunnett's test (**a**–**f**). **g**, PBMCs from healthy donors were activated with plate-bound anti-CD3 and anti-CD28 antibodies for seven days in the presence or absence of infliximab (10 μg ml^{-1}) or etanercept (4 μg ml^{-1}). Cell death was monitored by annexin V staining of CD8$^+$ T cells. Data are mean ± s.d. $n = 15$ healthy donors for anti-CD3/CD28 + etanercept; $n = 11$ for anti-CD3/CD28 + infliximab. *P* values were calculated using a two-sided paired *t*-test.

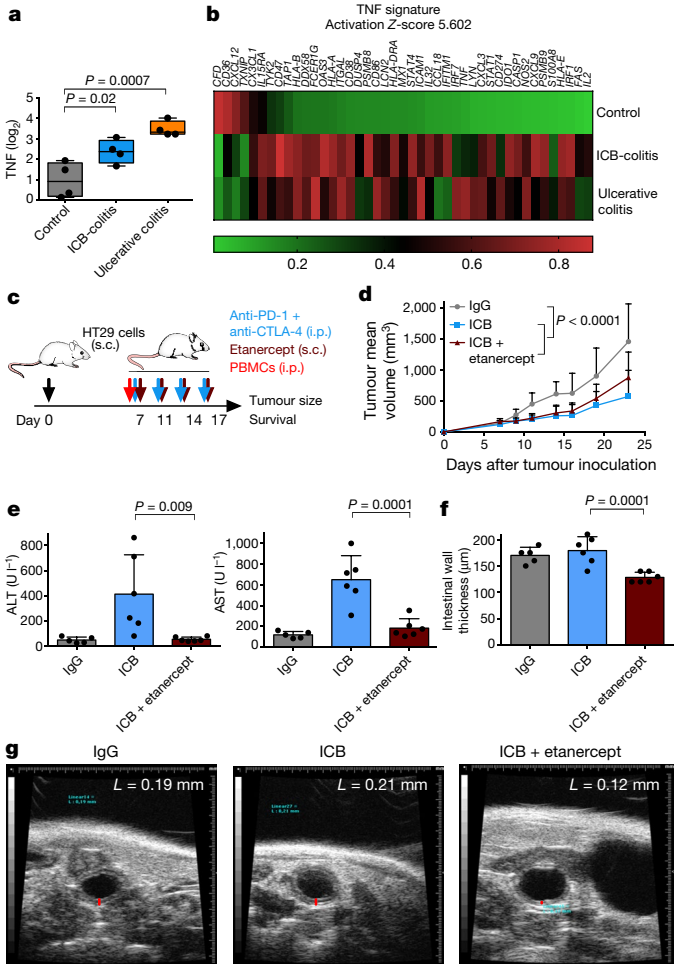

Fig. 4 | TNF is involved in immune checkpoint blockade-induced colitis in patients and in a humanized mouse model. Gene-expression profiling (using an nCounter Analysis System with the PanCancer Immune Profiling Panel set of probes) was performed in different samples of human mucosal tissue from colon biopsies: four samples of healthy mucosal tissue from the large intestine (control); samples from four cases of colitis induced by immune checkpoint blockade (ICB-colitis); and samples from four cases of ulcerative colitis. **a**, Gene expression of *TNF*. Centre line, median; box limits, 25th to 75th percentiles; whiskers, minimum and maximum values. $n = 4$ biologically independent patient samples. *P* values were calculated using a one-way ANOVA followed by Dunnett's test. **b**, Gene signature that denotes TNF activation in the ICB-colitis and ulcerative colitis groups versus the control group. Data are from a single experiment (**a**, **b**). **c**, Schematic representation of the treatments applied to immunodeficient *Rag2*$^{-/-}$*Il2rg*$^{-/-}$ mice that were first subcutaneously engrafted with HT29 colon carcinoma cells, followed by the infusion of human PBMCs after seven days. Mice were injected on days 7, 11, 14 and 17 intraperitoneally with combined ipilimumab and nivolumab, with or without etanercept (40 μg; given subcutaneously). As an antibody control, we used human polyclonal IgG. **d**, Mean tumour volumes. Data are mean ± s.d. $n = 5$ biologically independent mice for IgG; $n = 6$ for treated groups. *P* values were calculated using an extra sum-of-squares *F* test. **e**, Alanine transaminase (ALT) and aspartate transaminase (AST) serum levels on day 24. **f**, Ultrasound assessments of intestinal wall thickness on day 24. Data are mean ± s.d. $n = 5$ for IgG; $n = 6$ for treated groups. *P* values were calculated using a one-way ANOVA followed by Dunnett's test (**e**, **f**). **g**, Representative ultrasound images of the treatment groups described in **f**. Red bars indicate intestinal wall thickness. Data are from a single experiment.

Online content

Any methods, additional references, Nature Research reporting summaries, source data, statements of data availability and associated accession codes are available at https://doi.org/10.1038/s41586-019-1162-y.

Received: 14 September 2018; Accepted: 27 March 2019;
Published online 1 May 2019.

1. Wolchok, J. D., Rollin, L. & Larkin, J. Nivolumab and ipilimumab in advanced melanoma. *N. Engl. J. Med.* **377**, 2503–2504 (2017).
2. Motzer, R. J. et al. Nivolumab plus ipilimumab versus sunitinib in advanced renal-cell carcinoma. *N. Engl. J. Med.* **378**, 1277–1290 (2018).
3. Hellmann, M. D. et al. Nivolumab plus ipilimumab in lung cancer with a high tumor mutational burden. *N. Engl. J. Med.* **378**, 2093–2104 (2018).
4. Wolchok, J. D. et al. Nivolumab plus ipilimumab in advanced melanoma. *N. Engl. J. Med.* **369**, 122–133 (2013).
5. Curran, M. A., Montalvo, W., Yagita, H. & Allison, J. P. PD-1 and CTLA-4 combination blockade expands infiltrating T cells and reduces regulatory T and myeloid cells within B16 melanoma tumors. *Proc. Natl Acad. Sci. USA* **107**, 4275–4280 (2010).
6. Duraiswamy, J., Kaluza, K. M., Freeman, G. J. & Coukos, G. Dual blockade of PD-1 and CTLA-4 combined with tumor vaccine effectively restores T-cell rejection function in tumors. *Cancer Res.* **73**, 3591–3603 (2013).
7. Wainwright, D. A. et al. Durable therapeutic efficacy utilizing combinatorial blockade against IDO, CTLA-4, and PD-L1 in mice with brain tumors. *Clin. Cancer Res.* **20**, 5290–5301 (2014).
8. Spranger, S. et al. Mechanism of tumor rejection with doublets of CTLA-4, PD-1/PD-L1, or IDO blockade involves restored IL-2 production and proliferation of $CD8^+$ T cells directly within the tumor microenvironment. *J. Immunother. Cancer* **2**, 3 (2014).
9. Larkin, J. et al. Combined nivolumab and ipilimumab or monotherapy in untreated melanoma. *N. Engl. J. Med.* **373**, 23–34 (2015).
10. Ascierto, P. A. et al. Ipilimumab 10 mg/kg versus ipilimumab 3 mg/kg in patients with unresectable or metastatic melanoma: a randomised, double-blind, multicentre, phase 3 trial. *Lancet Oncol.* **18**, 611–622 (2017).
11. Postow, M. A. & Hellmann, M. D. Adverse events associated with immune checkpoint blockade. *N. Engl. J. Med.* **378**, 1163–1165 (2018).
12. Yamada, Y., Kirillova, I., Peschon, J. J. & Fausto, N. Initiation of liver growth by tumor necrosis factor: deficient liver regeneration in mice lacking type I tumor necrosis factor receptor. *Proc. Natl Acad. Sci. USA* **94**, 1441–1446 (1997).
13. Cooper, H. S., Murthy, S. N., Shah, R. S. & Sedergran, D. J. Clinicopathologic study of dextran sulfate sodium experimental murine colitis. *Lab. Invest.* **69**, 238–249 (1993).
14. Eichele, D. D. & Kharbanda, K. K. Dextran sodium sulfate colitis murine model: an indispensable tool for advancing our understanding of inflammatory bowel diseases pathogenesis. *World J. Gastroenterol.* **23**, 6016–6029 (2017).
15. Blonski, W., Buchner, A. M. & Lichtenstein, G. R. Treatment of ulcerative colitis. *Curr. Opin. Gastroenterol.* **30**, 84–96 (2014).
16. Popivanova, B. K. et al. Blocking TNF-α in mice reduces colorectal carcinogenesis associated with chronic colitis. *J. Clin. Invest.* **118**, 560–570 (2008).
17. Coward, J. et al. Interleukin-6 as a therapeutic target in human ovarian cancer. *Clin. Cancer Res.* **17**, 6083–6096 (2011).
18. Mace, T. A. et al. IL-6 and PD-L1 antibody blockade combination therapy reduces tumour progression in murine models of pancreatic cancer. *Gut* **67**, 320–332 (2018).
19. Bertrand, F. et al. TNFα blockade overcomes resistance to anti-PD-1 in experimental melanoma. *Nat. Commun.* **8**, 2256 (2017).
20. Hettich, M., Braun, F., Bartholomä, M. D., Schirmbeck, R. & Niedermann, G. High-resolution PET Imaging with therapeutic antibody-based PD-1/PD-L1 checkpoint tracers. *Theranostics* **6**, 1629–1640 (2016).
21. Kurtulus, S. et al. Checkpoint blockade immunotherapy induces dynamic changes in PD-1^-CD8^+ tumor-infiltrating T cells. *Immunity* **50**, 181–194.e6 (2019).
22. Siddiqui, I. et al. Intratumoral $Tcf1^+PD\text{-}1^+CD8^+$ T cells with stem-like properties promote tumor control in response to vaccination and checkpoint blockade immunotherapy. *Immunity* **50**, 195–211.e10 (2019).
23. Arakaki, R., Yamada, A., Kudo, Y., Hayashi, Y. & Ishimaru, N. Mechanism of activation-induced cell death of T cells and regulation of FasL expression. *Crit. Rev. Immunol.* **34**, 301–314 (2014).
24. Zheng, L. et al. Induction of apoptosis in mature T cells by tumour necrosis factor. *Nature* **377**, 348–351 (1995).
25. Sanmamed, M. F. et al. Nivolumab and urelumab enhance antitumor activity of human T lymphocytes engrafted in $Rag2^{-/-}IL2R\gamma^{null}$ immunodeficient mice. *Cancer Res.* **75**, 3466–3478 (2015).
26. Balkwill, F. Tumour necrosis factor and cancer. *Nat. Rev. Cancer* **9**, 361–371 (2009).
27. Madhusudan, S. et al. Study of etanercept, a tumor necrosis factor-alpha inhibitor, in recurrent ovarian cancer. *J. Clin. Oncol.* **23**, 5950–5959 (2005).
28. Harrison, M. L. et al. Tumor necrosis factor α as a new target for renal cell carcinoma: two sequential phase II trials of infliximab at standard and high dose. *J. Clin. Oncol.* **25**, 4542–4549 (2007).

Acknowledgements We thank M. Fernandez de Sanmamed and I. Etxeberria for scientific discussion, P. Miller for English editing and X. Morales for ultrasound imaging. The figures contain elements from Servier Medical Art (https://smart.servier.com/), licensed under Creative Commons Attribution 3.0 Unported License (https://creativecommons.org/licenses/by/3.0/). This work was supported by the International Immuno-Oncology Network (II-ON) from Bristol-Myers Squibb; a Worldwide Cancer Research Grant (15-1146); the Asociación Española Contra el Cancer (AECC) Foundation under grant GCB15152947MELE; the Instituto Carlos III (under grants PI14/01686, PI13/00207 and PI16/00668) co-financed with FEDER funds; and the European Union's Horizon 2020 Program (grant agreement no. 635122 PROCROP). P.B. is supported by a Miguel Servet II (CPII15/00004) contract from Instituto de Salud Carlos III; E.P.-R is supported by the Carmen Lavigne training program of the Asociación Española contra el Cancer and by Consejeria de Salud de la Junta de Andalucía; and A.T. has received financial support through la Caixa Banking Foundation (LCF/BQ/LR18/11640014).

Reviewer information *Nature* thanks Frances Balkwill, Kevin Tracey and the other anonymous reviewer(s) for their contribution to the peer review of this work.

Author contributions E.P.-R., L.M., P.B. and I.M. designed experiments. E.P.-R., V.B., C.M. and M.C.O. performed the in vivo experiments in Figs. 1, 2 and Extended Data Fig. 1. L.M. performed the experiments in Figs. 3a–f, 4c–g and Extended Data Fig. 8. I.O. performed the in vitro experiments with human PBMCs (Fig. 3g and Extended Data Fig. 7) and in vivo experiments with the anti-IL6 monoclonal antibody (Extended Data Fig. 2). Maite Alvarez performed the ELISA determinations in Extended Data Figs. 3, 4, and flow cytometry experiments in Extended Data Figs. 5, 6. A.T. contributed to the experiment in Extended Data Fig. 5. C.d.A. performed immunohistochemistry analysis and scored intestinal inflammation (Fig. 1e). M.E.R.-R., J.L.P.-G., I.M.-R. and C.L. provided human tissue samples (Fig. 4a, b). Martina Alvarez and V.D.L. performed NanoString analysis (Fig. 4a, b). L.M. and P.B. performed all statistical analyses. E.P.-R., L.M., P.B. and I.M. analysed the data. I.M. wrote the manuscript, assisted by E.P.-R, L.M. and P.B. for the figures. All authors performed a critical revision of the manuscript content and gave their final approval.

Competing interests I.M. reports advisory roles with Roche-Genentech, Bristol-Myers Squibb, CYTOMX, Incyte, MedImmune, Tusk, F-Star, Genmab, Molecular Partners, Alligator, Bioncotech, MSD, Merck-Serono and Bayer, and research funding from Roche, BMS, Alligator and Bioncotech. P.B. reports advisory roles with Tusk and Moderna, research funding from Sanofi, Moderna and Bavarian Nordic and speaker honoraria from BMS, MSD, Novartis and AstraZeneca. I.M.-R. reports advisory roles with Roche-Genentech, Bristol-Myers Squibb, Incyte, Merck, Amgen, Pierre Fabre, Novartis, and Bioncotech. J.L.P.-G. reports advisory roles with Roche, MSD and BMS, travel support from Roche, BMS and MSD and research funding from Roche, BMS, MSD, Ipsen, Eisai, Incyte and Janssen. E.P.-R. reports speaker honoraria and travel support from BMS, MSD and Novartis. The rest of the authors have no conflict of interest to declare.

Additional information

Extended data is available for this paper at https://doi.org/10.1038/s41586-019-1162-y.
Supplementary information is available for this paper at https://doi.org/10.1038/s41586-019-1162-y.
Reprints and permissions information is available at http://www.nature.com/reprints.
Correspondence and requests for materials should be addressed to P.B. or I.M.

METHODS

Mice and cell lines. Female C57BL/6 mice (6 weeks old) were obtained from the Jackson Laboratory and maintained in the animal facility of Cima Universidad de Navarra. *Rag2*$^{-/-}$*Il2rg*$^{-/-}$, OT-I and Pmel-1 mice were bred and maintained in the animal facility of Cima Universidad de Navarra. Experimental protocols were approved by the Ethics Committee of the Universidad de Navarra and the Institute of Public Health of Navarra according to European Council Guidelines (protocol numbers 060-17 and 024-17). Sample size estimations were performed using G Power software. Mice were randomized at the beginning of each experiment and experiments were not blinded. Mice were killed when tumours reached a mean diameter of 20 mm diameter, and this limit was not exceeded in any of the experiments. We complied with all ethical regulations. MC38 cells were a gift from K. E. Hellström (University of Washington) in September 1998. B16-OVA cells were provided by L. Chen (Yale University) in November 2001. These cell lines were authenticated by Idexx Radil (case 6592-2012) in February 2012. HT29 cells were obtained from ATCC. MC38, B16-OVA and HT29 cell lines were maintained at 37 °C in 5% CO_2 and were grown in RPMI medium (RPMI 1640) with Glutamax (Gibco; Invitrogen) containing 10% heat-inactivated fetal bovine serum (Gibco; Invitrogen), 100 IU ml^{-1} penicillin and 100 g ml^{-1} streptomycin (Biowhittaker). After seven to nine days in culture, cells were tested for mycoplasma contamination and 500,000 cells per mouse were injected subcutaneously. Tumour growth was monitored twice a week with an electronic caliper.

Treatments. Mice received 100 μg of anti-CTLA-4 antibody (InVivoMAb BioXCell; anti-mouse CTLA-4, clone 9D9) and 100 μg of anti-PD-1 antibody (InVivoMAb BioXCell; anti-mouse PD-1, clone RMP1-14) per injection intraperitoneally. Colitis treatment consisted of the intraperitoneal administration of anti-mouse TNF antibody (125 μg per injection per mouse; InVivoMAb BioXCell; clone XT3.11) as previously described[29], or etanercept (40 μg per injection per mouse; Enbrel). Anti-mouse IL-6 antibody (InVivoMAb BioXCell; clone MPF5-20F3) was administered intraperitoneally (250 μg per dose).

DSS-induced colitis. Mice were orally administered 3% DSS (36–50 kDa; MP Biomedicals) in their drinking water for three days to induce acute colitis. The experiments were performed in these conditions because a protocol reported previously[30], which included 3% DSS in water over seven days, proved to be very toxic and produced high mortality in our model.

Colitis assessment. Several different parameters were used for colitis assessment. Mouse weight was monitored daily. Colon ultrasound scans were performed on days 0 and 7 using a Vevo 770 ultrasound system (Visualsonics) equipped with a real-time micro-visualization scanhead probe (RMV-710 B) working at a frame rate of 110–120 frames per second. The nosepiece transducer used had a central frequency of 25 MHz, a focal length of 15 mm and 70 mm of nominal spatial resolution. Scans were performed by a trained technician and intestinal wall thickness was determined. For histological studies, paraffin-embedded colon sections (4 μm) from each animal were stained with H&E. Histological changes were graded as previously described[31]. In brief, histological scores were determined blindly, based on analysis of the inflammatory cell infiltrate and changes in intestinal architecture.

Inflammatory cell infiltrate scores were as follows: 0, regular infiltrate; 1, infiltration of the lamina propia; 2, cryptitis; 3, crypt abscesses, surface erosion or ulceration.

Intestinal architecture scores were as follows: 0, regular architecture; 1, irregular crypts or irregular villous surface; 2, crypt loss; 3, ulceration or granulation tissue.

Mouse lymphocyte survival study. For in vitro experiments, 1.5×10^6 splenocytes from 6–10-week-old male or female OT-I or Pmel-1 transgenic mice were isolated and activated with 25 ng ml^{-1} of SIINFEKL peptide (Invivogen) or 500 ng ml^{-1} of gp100 peptide (GenScript), respectively. Splenocytes were also treated with 6.6 μg ml^{-1} of anti-CTLA-4 plus 6.6 μg ml^{-1} of anti-PD-1, and 2.6 μg ml^{-1} of etanercept or 8.3 μg ml^{-1} of anti-TNF. After 72 h, survival was analysed by flow cytometry (BD FACSCanto II system; anti-CD8 BV510, clone 53-6.7 (Biolegend); anti-CD3 PeCy7, clone 17A2 (Biolegend); Zombie NIR (Biolegend)).

For in vivo experiments, MC38 tumours were implanted subcutaneously and treated as described above. Seven days after the start of treatment, tumours were removed and the survival of antigen-specific CD8$^+$ cells was analysed by flow cytometry in tumours and draining lymph nodes (BD FACSCanto II system; anti-CD8 BV510, clone 53-6.7 (Biolegend); anti-CD3 PeCy7, clone 17A2 (Biolegend); Zombie NIR (Biolegend); H-2K^b KSPWFTTL R-Pe-labelled Pro5 MHC Pentamer (ProImmune).

Human lymphocyte survival study. PBMCs from 21 healthy white donors (21–42 years old, males and females) were enriched using Ficoll-Paque Plus (GE Healthcare) and isolated by density-gradient centrifugation. All samples were obtained after consent from the healthy donors and Institutional Review Board approval from Clínica Universidad de Navarra, and we complied with all ethical regulations. PBMCs were stimulated with 0.5 μg ml^{-1} plate-bound anti-CD3 (OKT-3; eBioscience) and 1 μg ml^{-1} anti-CD28 (CD28.2; eBioscience) in the presence or absence of 10 μg ml^{-1} infliximab or 4 μg ml^{-1} etanercept. All cultures were carried out in the presence of 20 IU ml^{-1} recombinant human IL-2 (Proleukin; Novartis) in RPMI-10% fetal bovine serum at 37 °C. Seven days later, cells were replated into fresh anti-CD3 and anti-CD28-coated plates and cultured overnight in the presence of all stimuli. Cells were analysed by multicolour flow cytometry (BD FACSCanto II system; Zombie NIR (Biolegend); anti-CD3 PeCy7, clone UCHT1 (BD Biosciences; anti-CD8 BV510, clone BC96 (Biolegend); CD4–APC, clone OKT4 (Biolegend); annexin V FITC (Biolegend)). All analysis was performed using FlowJo 10.4.2 software (Tree Star).

NanoString and nCounter technology. For TNF signature analysis, we selected four mucosal biopsies from patients without bowel inflammation, four from patients with spontaneous active ulcerative colitis that was not associated with immunotherapy and four from patients who had immunotherapy-induced colitis. Among the immunotherapy-induced colitis patients, two were male and two were female, and there were two cases of grade 4 colitis refractory to corticosteroids. Two of the immunotherapy-related colitis cases occurred after treatment with ipilimumab and two after combined ipilimumab and nivolumab treatment. Among the four patients with spontaneous active ulcerative colitis, three were male and one female (20–69 years old). In the group without bowel inflammation, patients had colorectal adenocarcinoma, were 61–86 years old, and two were male and two female. Sample anonymization was performed by the corresponding biobanks. All biopsies were obtained after consent from the patients and after Institutional Review Board approval from Clínica Universidad de Navarra, Hospital General Universitario Gregorio Marañon and Hospital Universitario Virgen de la Victoria, and we have complied with all ethical regulations. A pathologist selected the formalin-fixed paraffin-embedded (FFPE) tumour block with the greatest area of viable normal mucosa of colon or ulcerative colitis, and estimated the tumour cellularity (>10%) and the tumour surface area within the circled area of the H&E-stained slide (>4 mm^2). FFPE samples were sent to the University of Málaga (CIMES) for macrodissection of material and RNA extraction using an RNA isolation kit and procedures provided by NanoString Technologies. The optical density of total RNA was measured at 260 nm and 280 nm to determine yield and purity. RNA samples were used if the measured concentration equalled or was higher than 12.5ng μl^{-1} and the absorbance ratio (260 nm/280 nm) was 1.7–2.5. Gene-expression profiling was performed on an nCounter Analysis System using the PanCancer Immune Profiling Panel set of probes (770 genes: 730 cancer-related human genes and 40 internal reference controls). The hybridization reaction was performed using a nominal RNA input of 250 ng. The hybridization time was 15–21 h, using a benchtop thermocycler set to 65 °C with a heated lid set to 70 °C. The manufacturer's specifications were followed for the nCounter Prep Station, which prepares the hybridized products for imaging. The nCounter Digital Analyzer reports the digital counts that represent the number of molecules labelled with a fluorescent barcode for each probe-targeted transcript. Data were analysed using nSolver software (Nanostring Technologies) and Ingenuity Pathway Analysis (Ingenuity Systems).

Xenograft-induced colitis experiment. On day 0, 8–12-week-old female *Rag2*$^{-/-}$*Il2rg*$^{-/-}$ mice were inoculated subcutaneously with 5×10^5 HT29 cells. On day 7 after tumour-cell inoculation, 10^7 human PBMCs resuspended in 1 ml PBS were injected intraperitoneally. Human blood samples were obtained from healthy donors, and fresh PBMCs were isolated by density-gradient separation (Ficoll Paque Plus; GE Healthcare).

On days 7, 11, 14 and 17, mice were injected intraperitoneally with ipilimumab (200 μg) and nivolumab (200 μg), and subcutaneously with etanercept (40 μg). As an antibody control, we used human IgG (200 μg). Ultrasound analyses of the intestine were performed on day 24, and photographs were obtained. Mice were bled on day 24 for serum collection. Transaminase analyses were performed on the Roche Cobas platform. Xenografted tumours were measured every three days.

Anti-drug antibody assay. MC38 tumour-bearing mice were treated with DSS with or without anti-TNF or etanercept. Serum samples were collected on days 4 and 8 after the beginning of treatment, and the samples were stored at −20 °C until analysis for anti-drug antibodies by an enzyme-linked immunosorbent assay (ELISA). In brief, 1:5 serially diluted serum samples, starting from a 1:10 dilution, were added to 96-well plates that were pre-coated with 0.1 μg in 50 μl of rat anti-TNF or etanercept, for the individual detection of anti-drug antibodies in serum from mice treated with DSS + ICB + anti-TNF or DSS + ICB + etanercept, respectively. As negative controls, sera collected from mice that were only treated with DSS were used. As a positive control, wells pre-coated in purified mouse IgG were used. To allow binding between the immobilized antibody and anti-drug antibodies, samples were incubated for 1.5 h at 37 °C, followed by thorough washing with PBS TWEEN 0.05% buffer (PBST) to eliminate unbound samples. Next, a highly cross-absorbed horseradish peroxidase (HRP)-labelled goat anti-mouse IgG (Life Technologies) was added at a 1:8,000 dilution and the samples were incubated for 1.5 h at 37 °C, followed by a thorough wash with PBST. HRP was detected by incubation with 3,3′,5,5′-tetramethylbenzidine substrate reagent (BD Biosciences) as per the manufacturer's instructions. The colorimetric reaction was measured in a spectrophotometer ($\lambda = 450$ nm). Data were represented by normalizing the

absorbance data from serum samples to the absorbance data obtained from the positive control. Half-maximal effective concentration (EC_{50}) values were calculated by a sigmoidal regression model.

TNF detection. To determine the levels of TNF protein in the tumour microenvironment, the tumour was first homogenized by mechanic disruption with a pestle in PBS buffer with complete protease inhibitors. After centrifugation, the supernatant was collected and stored at −20 °C for further use. Circulating TNF was measured in serum samples. 1:10 dilutions of tumour supernatant or 1:2 dilutions of serum were used to evaluate the levels of TNF protein, using the Mouse TNF ELISA Set II kit (BD OptEIATM) as per the manufacturer's instructions. The colorimetric reaction was measured in a spectrophotometer ($\lambda = 450$ nm).

List of antibodies used as T cell exhaustion-related markers. Anti-mouse eomesodermin (clone Dan11mag) eFluor 660, anti-mouse TIM3 (clone B8.2C12) PE/Dazzle 594, anti-human/mouse Tbet (clone eBio4B10) PECy7, anti-mouse CD45 (clone 30-F11) BV510, anti-mouse TCRβ (clone H57-597) BV610, anti-mouse CD19 (clone 6D5) BV660, anti-mouse CD8 (clone 53-6.7) BUV395, anti-mouse CD4 (clone GK1.5) BV496, anti-mouse FOXP3 (clone MF-14) BV421, anti-mouse Ki67 (clone 188A) Alexa Fluor 700, anti-mouse PD-1 (clone 29F.1A12), anti-mouse CTLA-4 (clone 1B8) FITC, anti-mouse LAG3 (clone C9B7W) PerCP-eFluor 510, anti-mouse 2B4 (clone m2B4-B6-4558.1) FITC, anti-mouse BTLA (clone 6F7) PerCP-eFluor 510, anti-mouse CD160 (clone CNX46-3) BV421, gp70 pentamer–PE, gp100 (KVPRNQDWL) pentamer–APC and OVA SIINFEKL) tetramer–PE. Stained cell suspensions were analysed by multicolour flow cytometry (Cytoflex, Beckman Coulter).

Statistical analysis. Prism software (GraphPad Software) was used for statistical analysis. We used the log-rank test to determine the significance of differences in survival curves. Mean differences were compared using *t*-tests (for comparisons of two groups) or one-way ANOVA followed by multiple-comparison tests (for comparisons of three of more groups). Longitudinal data were fitted to a third-order polynomial equation and compared with an extra sum-of-squares *F* test. *P* values <0.05 were considered to be statistically significant.

Reporting summary. Further information on research design is available in the Nature Research Reporting Summary linked to this paper.

Data availability

Source Data for all figures are provided.

29. Xiao, Y. T., Yan, W. H., Cao, Y., Yan, J. K. & Cai, W. Neutralization of IL-6 and TNF-α ameliorates intestinal permeability in DSS-induced colitis. *Cytokine* **83**, 189–192 (2016).
30. Mähler, M. et al. Differential susceptibility of inbred mouse strains to dextran sulfate sodium-induced colitis. *Am. J. Physiol.* **274**, G544–G551 (1998).
31. Tang, Q. et al. Role of far upstream element binding protein 1 in colonic epithelial disruption during dextran sulphate sodium-induced murine colitis. *Int. J. Clin. Exp. Pathol.* **7**, 2019–2031 (2014).

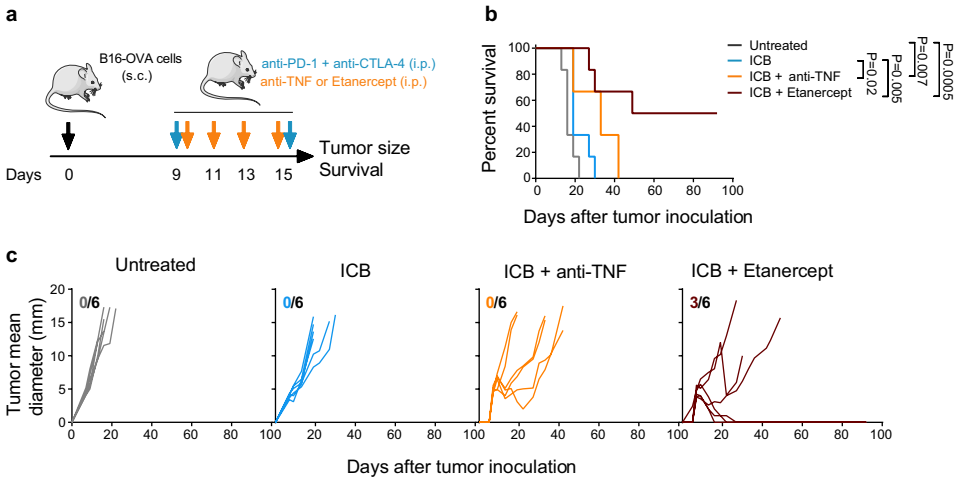

Extended Data Fig. 1 | Anti-tumour activity of double immune checkpoint blockade on B16-OVA-derived tumours on TNF blockade. **a**, Schematic representation of experiments. Experiments were performed as in Fig. 2a, but on mice bearing B16-OVA-derived tumours, treated in different groups. **b**, Overall survival of treatment groups. The numbers of biologically independent mice are indicated in **c**. *P* values were calculated using a two-sided log-rank test. **c**, Individual follow-up of tumour size, depicting the fraction of mice that completely rejected their tumours. One representative experiment out of two is shown.

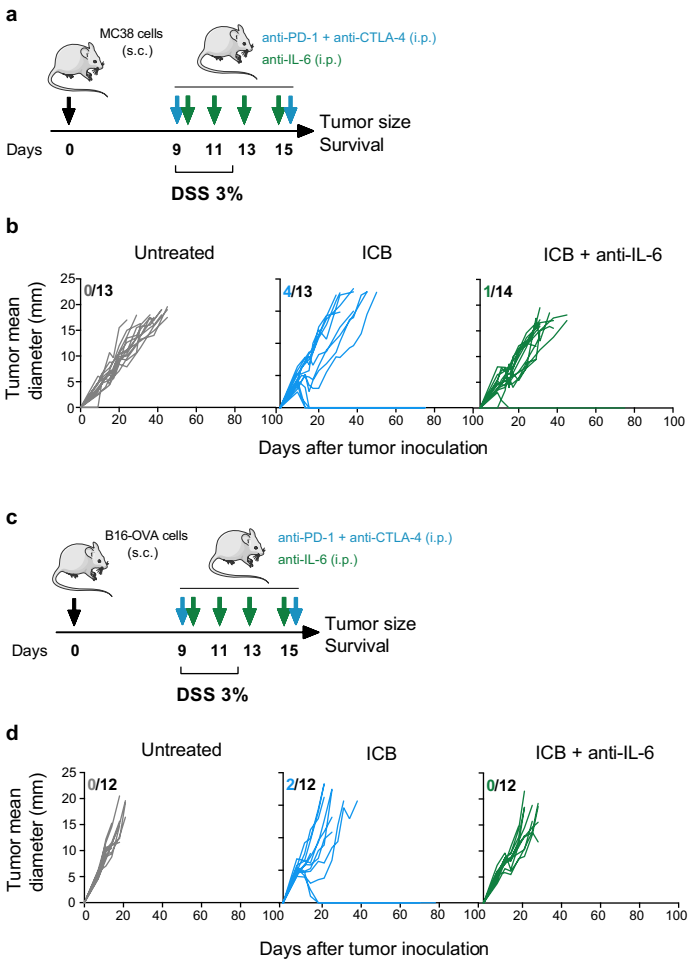

Extended Data Fig. 2 | Prophylactic IL-6 blockade hinders the anti-tumour activity of the combined anti-PD-1 and anti-CTLA-4 immunotherapy regimen. a, Schematic representation of the treatments applied to mice that were subcutaneously engrafted with MC38 colon carcinoma cells (the results from these mice are presented in **b**). **b**, Individual follow-up of tumour mean diameters, depicting the fraction of mice that completely rejected established tumours. **c**, Schematic representation of the treatments applied to mice that were subcutaneously engrafted with B16-OVA melanoma cells (the results from these mice are presented in **d**). **d**, Individual follow-up of tumour size, as in **b**. Data are pooled from two independent experiments.

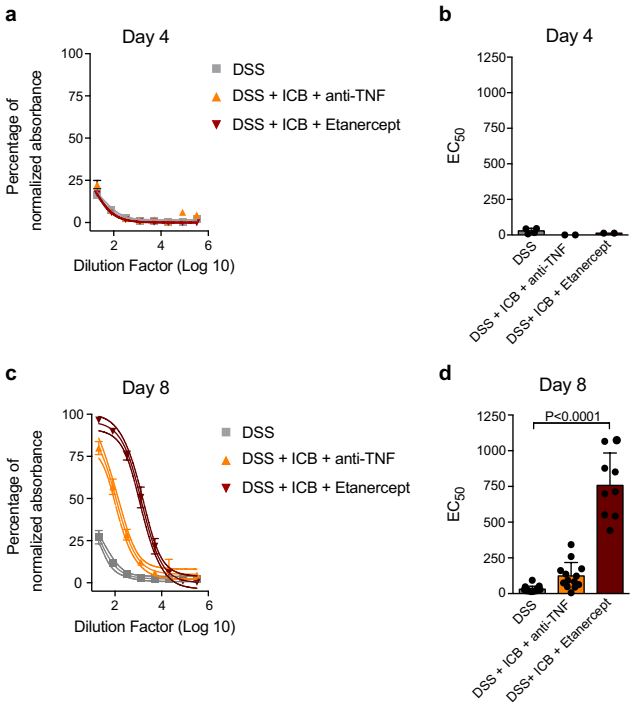

Extended Data Fig. 3 | Administration of etanercept causes mice to develop anti-drug antibodies. An assay to detect anti-drug antibodies was performed on serum that was collected from MC38 tumour-bearing mice 4 or 8 days after the start of treatment with TNF blockade (as in Fig. 2d). **a**, **c**, Percentages of normalized absorbance. Percentages reflect the levels of antibody against rat anti-TNF or anti-etanercept, as measured by ELISA on day 4 (**a**) and day 8 (**c**). **b**, **d**, EC_{50} values for day 4 (**b**) and day 8 (**d**). Data are mean ± s.d. $n = 15$ biologically independent mice for DSS, $n = 13$ for DSS + ICB + anti-TNF and $n = 9$ for DSS + ICB + etanercept. *P* values were calculated using a one-way ANOVA followed by Dunnett's test. A sigmoidal dose–response equation was used to determine EC_{50}. The continuous line represents the nonlinear regression curve fit, and the dotted line represents the s.d. Data are pooled from three independent experiments.

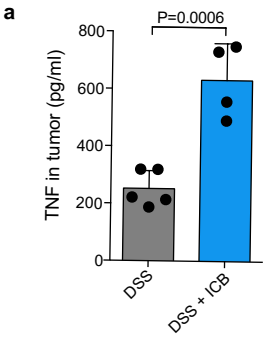

Extended Data Fig. 4 | Increased concentrations of TNF in the tumour microenvironment after immune checkpoint blockade therapy. Tumour homogenates were prepared from mice 24 h after they finished the treatment regimen described in Fig. 2d. Levels of TNF in the tumour are shown. Data are mean ± s.d. $n = 4$ biologically independent mice. *P* values were calculated using a two-sided *t*-test. TNF was undetectable in serum samples from the same mice. One representative experiment out of two is shown.

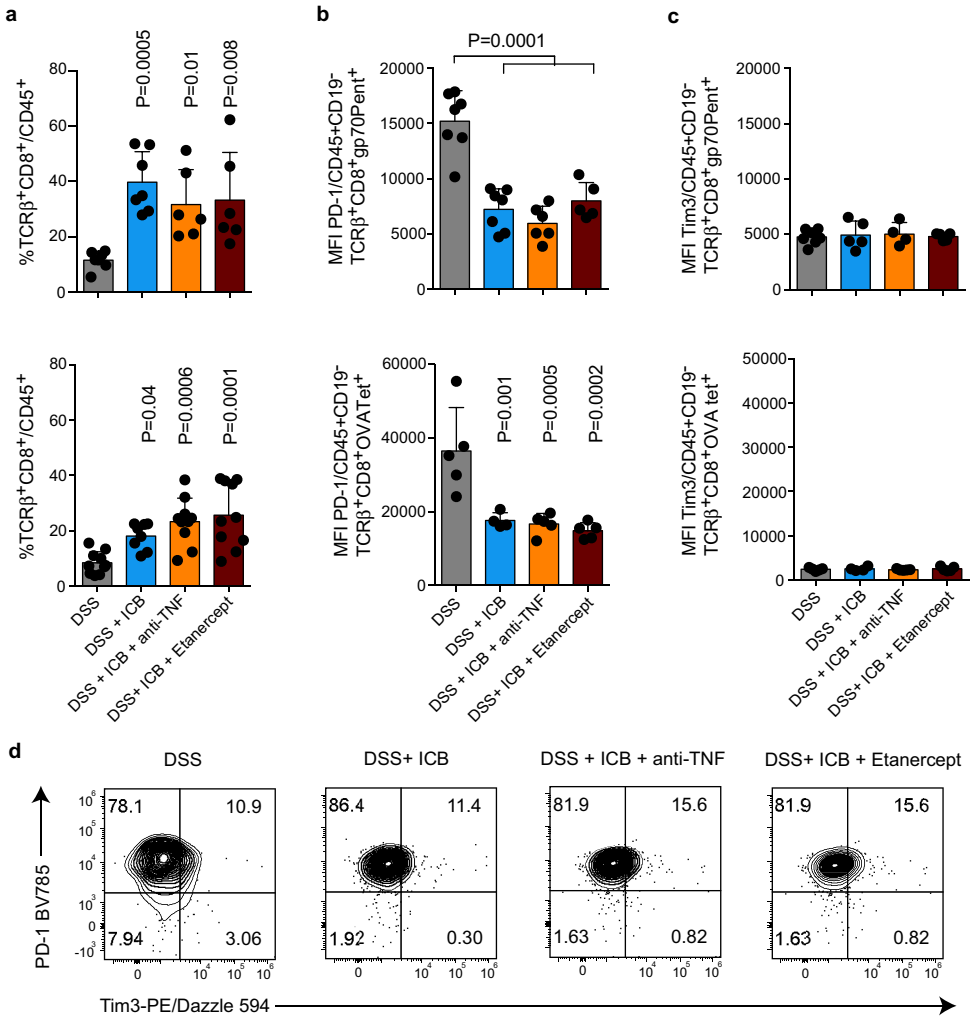

Extended Data Fig. 5 | Downregulation of PD-1 expression on tumour-infiltrating antigen-specific CD8$^+$ T cells following the combined anti-PD-1 and anti-CTLA-4 immunotherapy regimen. Tumours from MC38 and B16-OVA mouse models were collected 24 h after the mice finished the treatment regimen described in Fig. 2d, and cell suspensions were analysed by flow cytometry. **a**, The percentage of total TCRβ$^+$CD8$^+$ T cells among viable CD45$^+$ cells for MC38 (top) and B16-OVA (bottom) tumours. **b**, Median fluorescence intensity (MFI) of surface PD-1 for PD-1$^+$ cells previously gated on viable CD45$^+$CD19$^-$TCRβ$^+$CD8$^+$ gp70 pentamer$^+$ cells (top) or OVA tetramer$^+$ cells (bottom). **c**, MFI of surface TIM3 for TIM3$^+$ cells previously gated on viable CD45$^+$CD19$^-$TCRβ$^+$CD8$^+$gp70 pentamer$^+$ cells (top) or CD45$^+$CD19$^-$TCRβ$^+$CD8$^+$OVA tetramer$^+$ cells (bottom). Data are mean ± s.d. For the MC38 models (top), $n = 7$ biologically independent mice for DSS and DSS + ICB and $n = 6$ for the groups treated with anti-TNF or etanercept; for the B16-OVA models (bottom), $n = 6$ for DSS + ICB+ anti-TNF and $n = 10$ for the other groups. *P* values were calculated using a one-way ANOVA followed by Dunnett's test, and each condition was compared with the DSS group as a control. **d**, Representative contour plots of PD-1 and TIM3 in the experimental groups described in **b** for viable CD45$^+$CD19$^-$TCRβ$^+$CD8$^+$gp70 pentamer$^+$ cells. Fluorescence minus one (FMO) negative controls were used. Data are representative of two independent experiments.

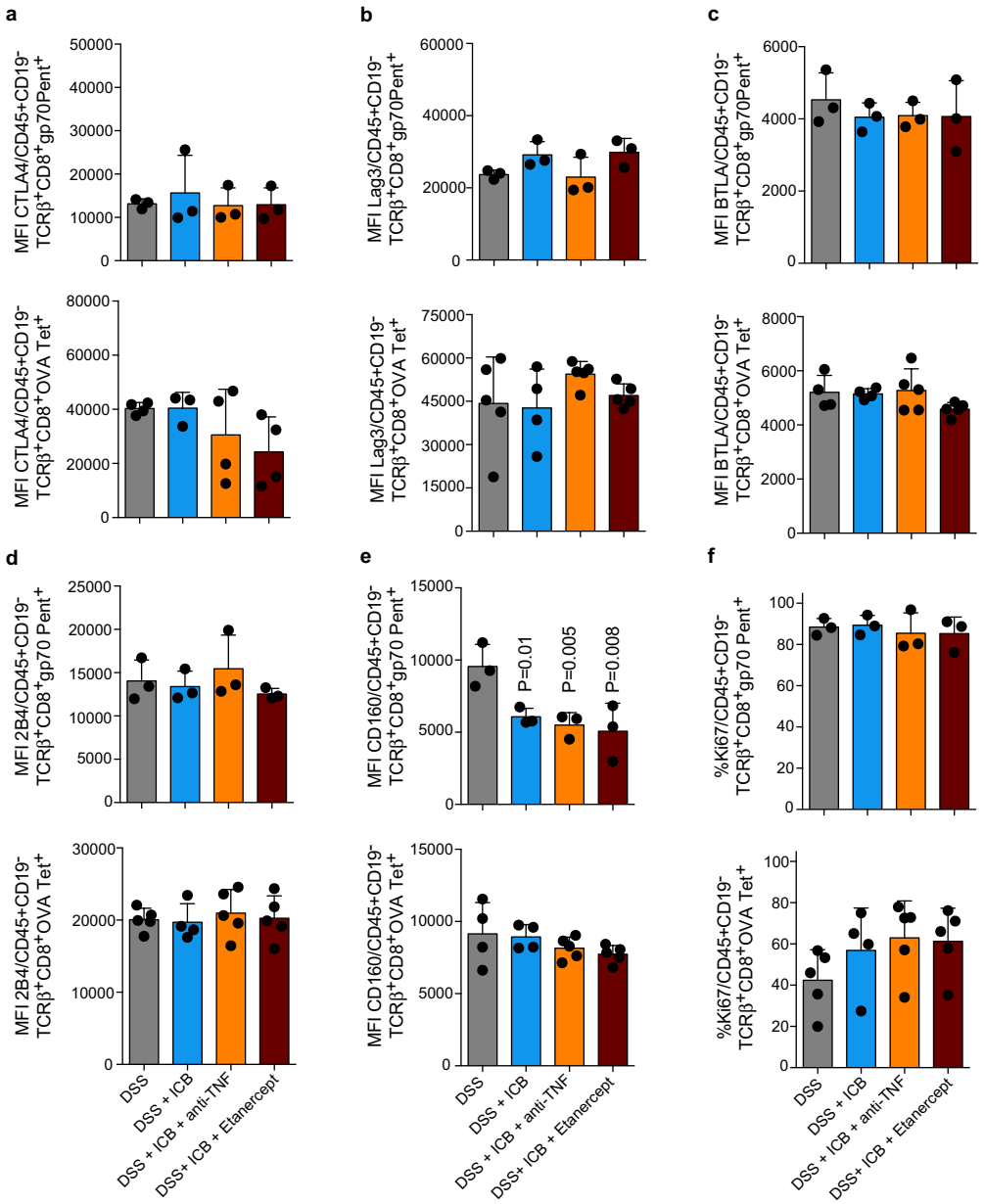

Extended Data Fig. 6 | Expression of T cell exhaustion-related markers on T cells following immune checkpoint blockade treatment with or without TNF blockade. a–f, Tumour-specific $CD8^+$ T cells recognizing gp70 (top) or OVA (bottom), in tumour-cell suspensions that were derived one day after completion of the indicated treatments, were analysed by multicolour flow cytometry. Expression of surface CTLA-4 (**a**), LAG3 (**b**), BTLA (**c**), 2B4 (**d**), CD160 (**e**) and intracellular Ki67 (**f**) are shown. Data are MFI (mean ± s.d.) for surface markers (**a**–**e**) and percentage of positive cells (mean ± s.d.) for Ki67 (**f**). For the MC38 models (top), $n = 3$; for the B16-OVA models (bottom), $n = 4$ for the DSS + ICB group and $n = 5$ for the other groups. *P* values were calculated using a one-way ANOVA followed by Dunnett's test, and each condition was compared with the DSS group as a control. Data are representative of two independent experiments.

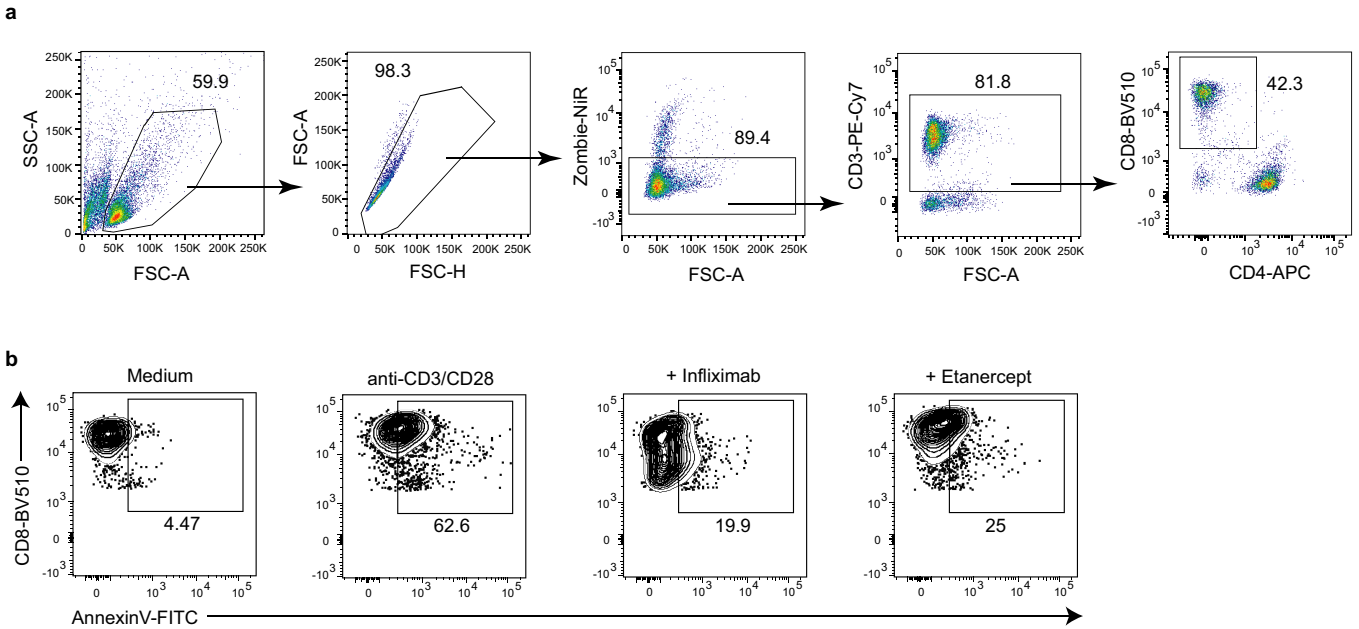

Extended Data Fig. 7 | Gating strategy and representative contour plots of AICD protection by TNF blockade in human PBMCs. **a**, Gating strategy for flow cytometry analysis. **b**, Representative contour plots showing annexin V-positive cells among $CD8^+$ T lymphocytes after stimulation with anti-CD3 and anti-CD28, with or without TNF blockade with infliximab or etanercept (the experimental groups are those described in Fig. 3g).

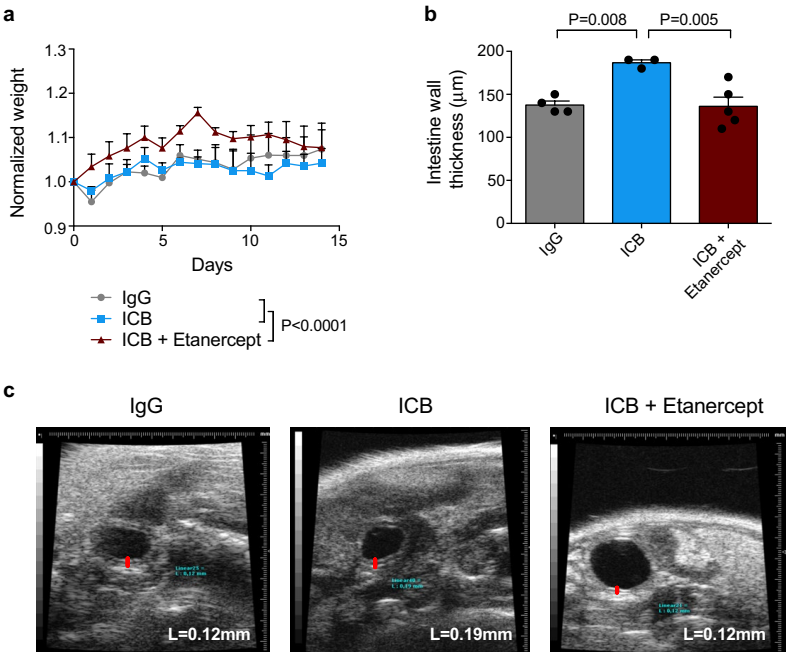

Extended Data Fig. 8 | The TNF axis is involved in immune-mediated colitis, as exacerbated by immune checkpoint blockade, in immune-deficient mice reconstituted with human PBMCs. Fresh human PBMCs were injected intraperitoneally on day 0 into immunodeficient *Rag2*$^{-/-}$*Il2rg*$^{-/-}$ mice. On days 0, 4, 7 and 10, mice were injected intraperitoneally with ipilimumab (200 μg) and nivolumab (200 μg), with or without etanercept (40 μg; given subcutaneously). As an antibody control, we used human polyclonal IgG. **a**, Normalized follow-up of body weight. Data are mean ± s.d. $n = 4$ biologically independent mice for all groups, except $n = 5$ for PBMCs + ICB + etanercept. *P* values were calculated using an extra sum-of-squares *F* test. **b**, Ultrasound assessments of intestinal wall thickness. Data are mean ± s.d. $n = 4$ biologically independent mice for PBMCs + IgG, $n = 3$ for PBMCs + ICB and $n = 5$ for PBMCs + ICB + etanercept. *P* values were calculated using a one-way ANOVA followed by Dunnett's-test. **c**, Representative ultrasound images estimating colon wall thickness in the different experimental groups described in **b**. Red bars indicate intestinal wall thickness. Data are from a single experiment.

nature research

Corresponding author(s): Pedro Berraondo and Ignacio Melero

Reporting Summary

Nature Research wishes to improve the reproducibility of the work that we publish. This form provides structure for consistency and transparency in reporting. For further information on Nature Research policies, see Authors & Referees and the Editorial Policy Checklist.

Statistical parameters

When statistical analyses are reported, confirm that the following items are present in the relevant location (e.g. figure legend, table legend, main text, or Methods section).

n/a	Confirmed	
☐	☒	The exact sample size (*n*) for each experimental group/condition, given as a discrete number and unit of measurement
☐	☒	An indication of whether measurements were taken from distinct samples or whether the same sample was measured repeatedly
☐	☒	The statistical test(s) used AND whether they are one- or two-sided *Only common tests should be described solely by name; describe more complex techniques in the Methods section.*
☐	☒	A description of all covariates tested
☐	☒	A description of any assumptions or corrections, such as tests of normality and adjustment for multiple comparisons
☐	☒	A full description of the statistics including central tendency (e.g. means) or other basic estimates (e.g. regression coefficient) AND variation (e.g. standard deviation) or associated estimates of uncertainty (e.g. confidence intervals)
☐	☒	For null hypothesis testing, the test statistic (e.g. *F*, *t*, *r*) with confidence intervals, effect sizes, degrees of freedom and *P* value noted *Give P values as exact values whenever suitable.*
☒	☐	For Bayesian analysis, information on the choice of priors and Markov chain Monte Carlo settings
☒	☐	For hierarchical and complex designs, identification of the appropriate level for tests and full reporting of outcomes
☒	☐	Estimates of effect sizes (e.g. Cohen's *d*, Pearson's *r*), indicating how they were calculated
☐	☒	Clearly defined error bars *State explicitly what error bars represent (e.g. SD, SE, CI)*

Our web collection on statistics for biologists may be useful.

Software and code

Policy information about availability of computer code

Data collection	GraphPad Prism® 7.01 (GraphPad Software, Inc., La Jolla, CA), Microsoft Excel 2010
Data analysis	GraphPad Prism® 7.01 (GraphPad Software, Inc., La Jolla, CA), nSolver 4.0 software (Nanostring Technologies, Seattle, WA), FlowJo 10.4.2 software (Tree Star, San Carlos, CA) and Ingenuity Pathway Analysis (Ingenuity Systems, Redwood City, CA).

For manuscripts utilizing custom algorithms or software that are central to the research but not yet described in published literature, software must be made available to editors/reviewers upon request. We strongly encourage code deposition in a community repository (e.g. GitHub). See the Nature Research guidelines for submitting code & software for further information.

Data

Policy information about availability of data

All manuscripts must include a data availability statement. This statement should provide the following information, where applicable:

- Accession codes, unique identifiers, or web links for publicly available datasets
- A list of figures that have associated raw data
- A description of any restrictions on data availability

All figures have associated raw data.

Field-specific reporting

Please select the best fit for your research. If you are not sure, read the appropriate sections before making your selection.

☒ Life sciences ☐ Behavioural & social sciences ☐ Ecological, evolutionary & environmental sciences

For a reference copy of the document with all sections, see nature.com/authors/policies/ReportingSummary-flat.pdf

Life sciences study design

All studies must disclose on these points even when the disclosure is negative.

Sample size	To calculate the sample size we used the computer application G Power software (http://www.gpower.hhu.de/).
Data exclusions	None
Replication	All studies have been repeated at least twice with similar results except experiments in Rag2-/-IL2Rγnull mice (that were performed with and without tumors) and NanoString data.
Randomization	The animals were randomly assigned to the groups.
Blinding	This manuscript focused on preclinical research. Assays were not blinded because the administration and sample collection and processing carried out by the same researchers.

Reporting for specific materials, systems and methods

Materials & experimental systems

n/a	Involved in the study
☒	☐ Unique biological materials
☐	☒ Antibodies
☐	☒ Eukaryotic cell lines
☒	☐ Palaeontology
☐	☒ Animals and other organisms
☐	☒ Human research participants

Methods

n/a	Involved in the study
☒	☐ ChIP-seq
☐	☒ Flow cytometry
☒	☐ MRI-based neuroimaging

Antibodies

Antibodies used	Anti-CTLA-4 antibody (InVivoMAb BioXCell anti-mouse CTLA-4, Clone 9D9), anti-PD-1 antibody (InVivoMab BioXCell anti-mouse PD-1, Clone RMP1-14), anti-mouse TNF-α antibody (InVivoMAb BioXCell, Clone XT3.11, eBioscience, San Diego, CA), Etanercept (Enbrel®), anti-CD8 BV510 clone 53-6.7 Biolegend, anti- CD3 PeCy7 clone 17A2 Biolegend, R-Pe Labelled Pro5 MHC Pentamer ProImmune, anti-PD-1 FITC clone 29F.1A12 Biolegend, anti-TIM-3 PerCP/Cy5.5 clone RMT3-23 Biolegend.
Validation	All antibodies were commercially available and validation can be found in the respective webpage.

Eukaryotic cell lines

Policy information about cell lines

Cell line source(s)	MC38 cells were a kind gift from Dr. Karl E. Hellström (University of Washington, Seattle, WA) in September 1998. B16-OVA cells were provided by Dr. Lieping Chen (Yale University, New Haven, CT) in November 2001. HT29 were obtained from ATCC.
Authentication	MC38 and B16-OVA cell lines were authenticated by Idexx Radil (Case 6592-2012) in February 2012.
Mycoplasma contamination	All cell lines were tested negative for mycoplasma contamination.
Commonly misidentified lines (See ICLAC register)	We did not used commonly misidentified lines.

Animals and other organisms

Policy information about studies involving animals; ARRIVE guidelines recommended for reporting animal research

Laboratory animals	6 week-old female C57BL/6 mice were obtained from The Jackson Laboratory (Bar Harbor, ME) and maintained in the animal facility of the Cima Universidad de Navarra. 6-10 week-old male or female OT-I transgenic mice, 6-10 week-old male or female Pmel-1 transgenic mice and 8-12 week-old female Rag2-/-IL2Rγnull were bred and maintained in the animal facility of Cima Universidad de Navarra. Experimental protocols were approved by the Ethics Committee of the University of Navarra and the Institute of Public Health of Navarra according to European Council Guidelines (protocol numbers: 060-17 and 024-17).
Wild animals	The study did not involve wild animals.
Field-collected samples	The study did not involve samples collected from the field.

Human research participants

Policy information about studies involving human research participants

Population characteristics	For TNF signature analysis, we selected four mucosal biopsies from patients without bowel inflammation, four from patients with spontaneous active ulcerative colitis that was not associated with immunotherapy and four from patients who had immunotherapy-induced colitis. Among the immunotherapy-induced colitis patients, two patients were male and two were female, and there were two cases of grade 4 colitis refractory to corticosteroids. Two of the immunotherapy-related colitis cases occurred after treatment with ipilimumab and two after combined ipilimumab and nivolumab treatment. Among the four patients with spontaneous active ulcerative colitis, three were male and one female (20–69 years old). In the group without bowel inflammation, patients had colorectal adenocarcinoma, were 61–86 years old, and two were male and two female. Sample anonymization was performed by the corresponding biobanks. All biopsies were obtained after consent from the patients and Institutional Review Board approval from Clínica Universidad de Navarra, Hospital General Universitario Gregorio Marañon and Hospital Universitario Virgen de la Victoria. PBMCs were obtained from 21 healthy white donors (21-42 years, males and females) were enriched using Ficoll-Paque Plus (GE Healthcare, Menlo Park, CA) and isolated by density gradient centrifugation. All samples were obtained after consent from the healthy donors and Institutional Review Board approval from Clínica Universidad de Navarra and we have complied with all ethical regulations.
Recruitment	A pathologist selected the FFPE tumor block with the greatest area of viable normal mucosa of colon or ulcerative colitis and estimated tumor cellularity (> 10%) and tumor surface area within the circled area of the H&E-stained slide (> 4 mm2).

Flow Cytometry

Plots

Confirm that:

☒ The axis labels state the marker and fluorochrome used (e.g. CD4-FITC).

☒ The axis scales are clearly visible. Include numbers along axes only for bottom left plot of group (a 'group' is an analysis of identical markers).

☒ All plots are contour plots with outliers or pseudocolor plots.

☒ A numerical value for number of cells or percentage (with statistics) is provided.

Methodology

Sample preparation	Spleens, draining lymph nodes or tumors were mechanically dissociated. Tumor suspensions were treated with DNAse and collagenase.
Instrument	FACSCanto™ II (Beckman Coulter) and Cytoflex (Beckman Coulter)
Software	FlowJo 10.4.2 (Tree Star, Ashland, OR)
Cell population abundance	N.A.
Gating strategy	N.A.

☒ Tick this box to confirm that a figure exemplifying the gating strategy is provided in the Supplementary Information.